Surface Science 687 (2019) 48–55

Contents lists available at ScienceDirect

Surface Science

journal homepage: www.elsevier.com/locate/susc

Anisotropic work function of elemental crystals

Richard Tran[a], Xiang-Guo Li[a], Joseph H. Montoya[b], Donald Winston[b], Kristin Aslaug Persson[b,c], Shyue Ping Ong[*,a]

[a] Department of NanoEngineering, University of California San Diego, 9500 Gilman Dr, Mail Code 0448, La Jolla, CA 92093-0448, United States
[b] Environmental Energy Technologies Division, Lawrence Berkeley National Laboratory, Berkeley, CA 94720, United States
[c] Department of Materials Science & Engineering, University of California Berkeley, Berkeley, CA 94720-1760, United States

ARTICLE INFO

Keywords:
DFT
Work function
Smoluchowski smoothing
Surface energy
Wulff shape
High-throughput workflow

ABSTRACT

The work function is a fundamental electronic property of a solid that varies with the facets of a crystalline surface. It is a crucial parameter in spectroscopy as well as materials design, especially for technologies such as thermionic electron guns and Schottky barriers. In this work, we present the largest database of calculated work functions for elemental crystals to date. This database contains the anisotropic work functions of more than 100 polymorphs of about 72 elements and up to a maximum Miller index of two and three for non-cubic and cubic crystals, respectively. The database has been rigorously validated against previous experimental and computational data where available. We also propose a weighted work function based on the Wulff shape that can be compared to measurements from polycrystalline specimens, and show that this weighted work function can be modeled empirically using simple atomic parameters. Furthermore, for the first time, we were able to analyze simple bond breaking rules for metallic systems beyond a maximum Miller index of one, allowing for a more generalized investigation of work function anisotropy.

1. Introduction

The work function (Φ) is an electronic surface property of crystalline solids and is crucial to the understanding and design of materials in many applications. It can be directly applied to the engineering of device specifications such as the Schottky barrier of semiconductor junctions or the thermionic currents of electron guns. Furthermore, it has been used to guide the engineering of interfacial interactions between metals and monolayer structures for nanoscale self-assembly [1]. The work function is also an important parameter in characterization techniques where it can influence the tip tunneling current of scanning tunneling microscopes or correct the binding energy in photo-electron spectroscopy (PES).

The work function has also been explored as a parameter for materials design. For example, previous experimental and computational investigations of Ni-alloys by Lu et al. [2,3] have established a correlation between the work function and various mechanical properties such as toughness, hardness, ductility and bulk modulus. A more recent study using first-principle calculations found similar correlations for elemental crystalline solids [4]. The work function has also been proposed as a possible parameter for the desorption rate of surface adsorbates [5]. Calculated work functions of hcp materials have also been used to screen for more effective metallic photocathodes [6].

Much effort has also been devoted to modelling Φ itself. Michaelson [7] and Miedema et al. [8], for example, were previously successful in modelling the polycrystalline work function as a linear function of electronegativity. The modeling of the anisotropic work function (Φ_{hkl}) as a function of surface morphology and chemical environment has also garnered much attention. Smoluchowski smoothing is one such model which describes the contributions to the work function of metals as a result of isotropic electron spreading and anisotropic electron smoothing [9]. The spreading of negative charges increases the work function while the anisotropic smoothing of negative charges at the surface decreases the work function. Smoothing increases with surface roughness (defined here as the reciprocal of the surface packing fraction [10]) which decreases the work function. This model is supported by previous observations that the anisotropic surface energy (γ_{hkl}) is inversely proportional to Φ_{hkl} via the broken bond surface density [11,12]. Similarly, the Brodie model attempts to explain Φ_{hkl} for transition metals as a function of (bulk) electron effective mass, surface atomic radius and inter-planar distance [13,14]. A more recent model using a dielectric formalism has been proposed by Fazylov [15] that describes Φ_{hkl} using surface roughness and surface plasmon dispersion.

An extensive database for Φ_{hkl} would be invaluable for validating

* Corresponding author.
E-mail address: ongsp@eng.ucsd.edu (S.P. Ong).

https://doi.org/10.1016/j.susc.2019.05.002
Received 15 February 2019; Accepted 11 May 2019
Available online 12 May 2019
0039-6028/

and further expanding upon these models. However, experimentally measured work functions are usually for polycrystalline specimens (Φ_{poly}^{expt}) instead of single crystals. An example of this is the extensive collection of experimentally measured Φ_{poly}^{expt} for 66 polycrystalline elemental solids compiled by Michaelson [16]. Though measurements for anisotropic Φ_{hkl} are not uncommon, values often vary due to the many techniques used or non-standardized methods of implementing the same technique (e.g., PES) [17,18]. The sparsity of Φ_{hkl} and the lack of a comprehensive compilation with a single standardized technique makes it difficult to develop and gain insights into work function anisotropy using experimental measurements.

Here, density functional theory (DFT) has the advantage of calculating Φ_{hkl} for a model of any specific solid surface under a controllable set of parameters, making it possible to create a standardized collection of values. Many authors have attempted such compilations for Φ_{hkl}, which are often times accompanied by the corresponding surface energy γ_{hkl} [11,12,19–22]. For instance, Ji et al. [12] and Wang and Wang [11] have calculated Φ_{hkl} for numerous bcc, fcc and hcp materials. Waele et al. [21] created a database of Φ_{hkl} for all elemental crystalline solids, but only for facets up to a max Miller index (MMI) of 1, using the Perdew-Burke-Ernzerhof generalized gradient approximation (PBE-GGA) and localized density approximation (LDA) functionals. More recently, Patra et al. [23] evaluated the performance of various functionals by calculating Φ_{hkl} for an MMI of one for Al, Cu, Ru, Rh, Pd, Ag, Pt and Au. Despite the wide variety of computational data, the majority of these studies are limited to small Miller indices (typically MMI of 1). In addition, computational data for lanthanide systems and different polymorphs is sparse [22,24,25]. Furthermore, most compilations do not consider possible reconstructions, which can drastically affect the calculated work function [21].

Here, we report the development of a comprehensive, validated database of work functions for elemental crystalline solids using DFT calculations that addresses all the above limitations in the following ways:

1. Coverage of 142 polymorphs of 72 elements, including rare earth metals.
2. Facets up to an MMI of three and two for cubic and non-cubic crystals, respectively, are considered.
3. Common reconstruction schemes, such as the missing-row (110) fcc and the diamond-type reconstructions, [26] have been taken into account.

We validate our computed work functions with past experimental and computational data for both Φ_{hkl} and Φ_{poly}^{expt}. Finally, we will discuss trends in the work function of the elements, and develop a predictive empirical model for Φ_{poly}^{expt}.

2. Methods

2.1. Definitions

The work function is defined as the energy barrier required to move an electron from the surface of a solid material into free space, as given by the following expression:

$$\Phi = V_{vac} - E_F \tag{1}$$

where V_{vac} is the electrostatic potential of the vacuum region near the surface and E_f is the Fermi energy of the slab. The energy barrier can be visualized in Fig. 1 where V_{vac} is obtained when the electron is far enough away from the surface, that the potential remains constant over a small distance in the vacuum. This method has been widely used in previous studies for calculating the work function [11,12,21,22] and has been shown to converge quickly with respect to slab thickness [19].

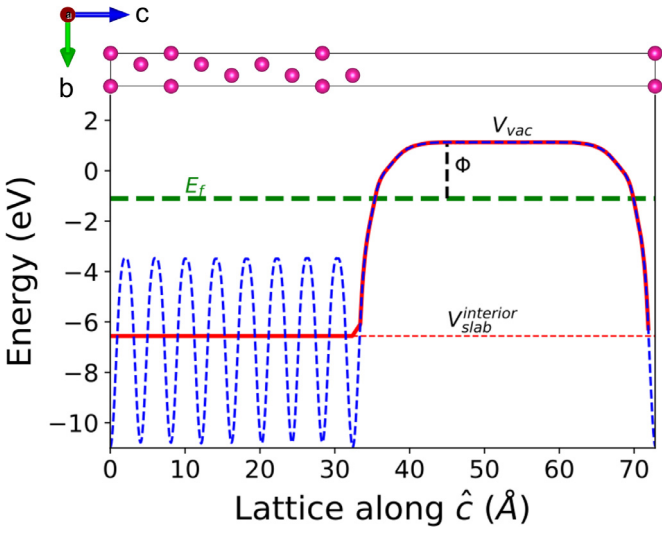

Fig. 1. Plot of the electrostatic potential along the hcp Rb (0001) slab model. The Fermi energy (E_f), electrostatic potential of the vacuum region (V_{vac}), average electrostatic potential of the slab region ($V_{slab}^{interior}$) and work function (Φ) are indicated.

2.2. Modeling non-uniform work functions

For comparison to work functions obtained from polycrystalline specimens, one approach is to calculate the work function of a "patchy" surface by weighting each Φ_{hkl} by the area fraction of its corresponding facet [5,27] as follows:

$$\bar{\Phi} = \frac{\sum_{\{hkl\}} \Phi_{hkl} A_{hkl}}{\Sigma A_{hkl}} = \sum_{\{hkl\}} \Phi_{hkl} f_{hkl}^{A} \tag{2}$$

where A_{hkl} and f_{hkl}^{A} are the total area and the area fraction of all facets in the $\{hkl\}$ family, respectively. A polycrystal is an extreme case of a patchy surface, and as such the same technique can be applied to Φ_{poly}^{expt}. The PES signal of the patch with a lower work function will tend to eclipse those with higher work functions leading to an underestimated measurement of Φ_{poly}^{expt}. Thus, experimental values of the lowest anisotropic work function (Φ_{hkl}^{lowest}) are only ~ 90 meV lower than Φ_{poly}^{expt}. Because of this, it has also been suggested that Φ_{hkl}^{lowest} is a good estimate of Φ_{poly}^{expt} [5,18,21]. In this study, we use the facets present in the Wulff shape previously calculated by the current authors [28] as an estimate of the orientation and area fraction present in a polycrystalline sample to obtain $\bar{\Phi}$ and Φ_{hkl}^{lowest} as estimates for Φ_{poly}^{expt}.

As mentioned earlier, Smoluchowski smoothing describes the anisotropic work function of metals as being inversely correlated with the broken bonds per surface area. As such, we model our values for Φ_{hkl} normalized by $\bar{\Phi}$ using the ratio of broken bonds-to-bulk coordination number ($\frac{N_{BB}}{CN_{bulk}}$) in a slab normalized by the surface area-to-atomic area ratio ($\frac{A_{surf}}{\pi r_A^2}$) in order to compare across all systems:

$$\overline{BB} = \frac{N_{BB}}{CN_{bulk}} \times \frac{A_{surf}}{\pi r_A^2} \tag{3}$$

It is known that for bcc and hcp materials, the first nearest neighbors (1NN) and second nearest neighbors (2NN) are in close proximity to each other, leading to contributions from the latter to the anisotropy of surface energy [29]. Hence, when defining $\overline{BB}$ for a material, we will limit the maximum coordination number to the 1NN for fcc materials and explore both 1NN and 2NN for hcp and bcc materials. For hcp structures, we omitted Φ_{0001} when investigating the effect of the 1NN as the number of broken bonds will always be 0 which is unphysical. The inverse correlation between $\overline{BB}$ and Φ_{hkl} for each element can be quantified by the Pearson correlation coefficient (r). We will define systems with a negative linear trend between Φ_{hkl} and the normalized

broken bonds with $r < -0.75$ as having a strong correlation, $-0.75 < r < -0.5$ as having a moderate correlation and $r > -0.5$ as having a weak correlation. Only ground state metallic fcc, bcc and hcp systems were explored under this context.

2.3. Computational details and workflow

For all slab calculations, we performed a full relaxation of the site positions under a fixed volume before obtaining the electrostatic potential of the slabs (see ref [28] for a complete description of computational details). The electrostatic potentials only contains the electrostatic contributions (no contributions from the exchange correlation). All calculations were performed using the Vienna Ab initio Simulation Package (VASP) with the exchange-correlation effects modeled using the PBE-GGA functional. Calculations using the revised PBE (rPBE) functional were performed on a smaller set of data using the same parameters for comparison.

We used the high-throughput workflow proposed by Sun and Ceder [30] and implemented by Tran et al. [28] and Montoya and Persson [31] to obtain all required data. The workflow was implemented using the open-source software packages Python Materials Genomics, [32] FireWorks [33] and Atomate [34]. The work function is extracted from the calculations and inserted into the same database. To handle errors that may arise during calculations, the custodian software package was used as a wrapper around VASP together with a set of robust error handling rules. The database will be continuously improved and will continue growing as more structural data becomes available on the Materials Project [35].

2.4. Data availability

The data can be accessed from the elemental-surface-data-focused Crystalium [36] website, as well as from the Materials Project website [37] on its detail pages for specific crystals.

3. Results

Due to the vast number of data points for Φ_{hkl} when comparing to literature values, we have adopted a consistent marker shape and color scheme for ease of reference (see Fig. 2) for all subsequent plots. The shape and color represents the row and group of the element in the periodic table, respectively.

All values for Φ reported in this study, including those found in the literature, are listed in the Supplementary Information in Tables S1 and S2. Literature values for Φ were taken from the most recent experimental and computational studies available during the writing of this manuscript. Experimental values are explicitly annotated with a "expt" superscript, e.g., Φ_{poly}^{expt}, and unless otherwise indicated, all other values are computed values.

3.1. Experimental and computational validation

Figs. 3 shows a single-parameter $y = x + c$ least squares fit for $\bar{\Phi}$ vs Φ_{poly}^{expt} and Φ_{hkl}^{lowest} vs Φ_{poly}^{expt} for the ground state polymorph of each element. We find that the PBE $\bar{\Phi}$ are on average 0.31 eV closer to Φ_{poly}^{expt} than the PBE Φ_{hkl}^{lowest}. The linear fit for $\bar{\Phi}$ vs Φ_{poly}^{expt} also yielded a higher R^2 of 0.927 and a lower standard error of the estimate (SEE) of 0.246 eV compared to that of Φ_{hkl}^{lowest} vs Φ_{poly}^{expt} (R^2 = 0.862 eV and SEE = 0.339 eV). We find that $\bar{\Phi}$ systematically underestimates Φ_{poly}^{expt} by 0.18 eV on average. Notable outliers include $\Phi_{poly}^{expt,As}$ which is underestimated, and $\Phi_{poly}^{expt,La}$ and $\Phi_{poly}^{expt,Se}$ which are overestimated by more than the SEE. The largest error is for La, with an error of 0.86 eV. Although the Michaelson [16] values of $\Phi_{poly}^{expt,Re}$ is 0.44 eV closer to our calculated value, the more recent value reported by Kawano [5] is reported here.

Fig. 4 compares the facet-dependent work functions obtained in this study to values obtained experimentally from single crystals and from other functionals, including LDA, PBE and RPBE. Again, we find that the experimental values in Fig. 4(a) are on average 0.30 eV higher than the computed ones with an increasing deviation for work functions of lower values. The (100), (310) and (311) facets of the early transition and refractory metals (Mo, W and Nb) have some of the lowest work functions, which also have the greatest deviation between the PBE and experimental values. For the same elements, facets with higher work functions have a smaller deviation ((110) and (210)). An exception to this is Φ_{111}^{Ta} where computed and experimental values are in relative agreement despite having a value lower than other work functions. Meanwhile, the computed value of $\Phi_{0001}^{Graphite}$ greatly overestimates the experimental value (see ref [5]). In general, the qualitative trends in work functions for different facets of each element are in agreement with the experimental trends, with the notable exception of Al. Eastmen and Mee [40] previously reported the order of Φ_{hkl}^{Al} to be $\Phi_{111}^{Al} > \Phi_{100}^{Al} > \Phi_{110}^{Al}$ which is typical of fcc metals while a later work by Grepstad et al. [41] reported that $\Phi_{100}^{Al} > \Phi_{110}^{Al} \sim \Phi_{111}^{Al}$, which is consistent with our results (see Table S2 for values).

Our values for Φ_{hkl} are in excellent agreement with those calculated using PBE, LDA and RPBE (as shown in Fig. 4(b), (c) and (d) respectively) with values of R^2 greater than 0.94 in all three cases. Unsurprisingly, there is smaller deviation when comparing our data to other GGA values (0.11 eV for PBE and 0.06 eV for rPBE) than to LDA values which are on average 0.38 eV higher. The major discrepancy between PBE and rPBE are for the (0001) surfaces of Y, Sc and Zn, with the PBE values being higher by 0.34 eV, 0.27 eV and 0.29 eV, respectively. Our values for $\Phi_{21\bar{3}1}^{Sc}$ and Φ_{210}^{Ba} are significantly lower when compared to PBE values obtained from the literature. Overall, the LDA-computed work functions are on average closer to the experimental values with a deviation of 0.11 eV (see Fig. S1).

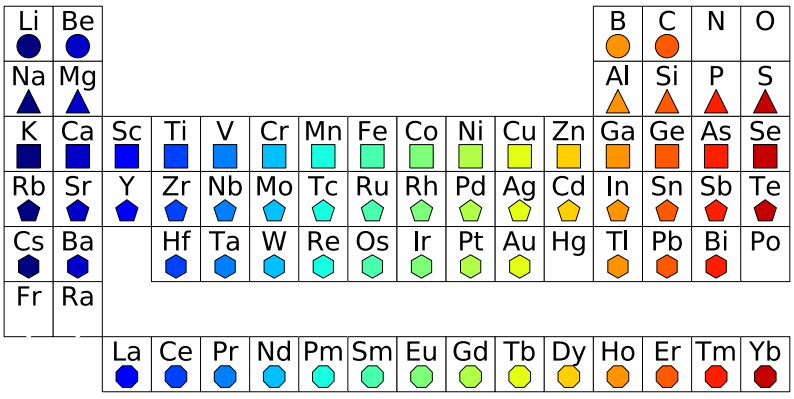

Fig. 2. Marker shape and color scheme for plots.

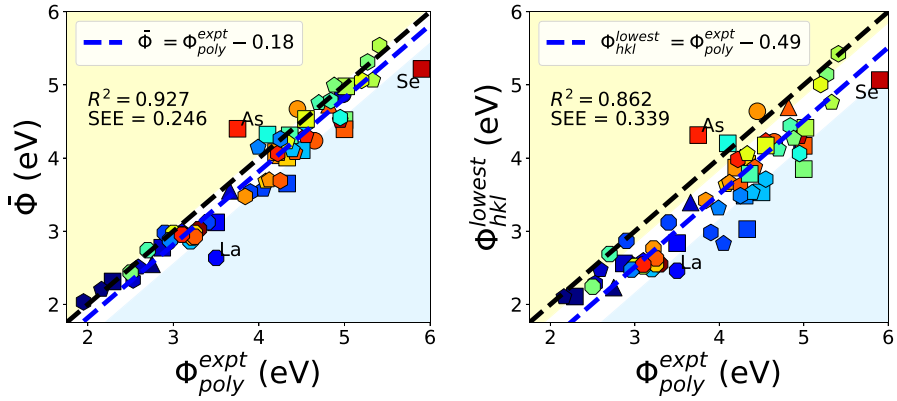

(a) $\Phi^{\text{expt}}_{\text{poly}}$ vs $\bar{\Phi}$ (b) $\Phi^{\text{expt}}_{\text{poly}}$ vs $\Phi^{\text{lowest}}_{\text{hkl}}$

Fig. 3. Plot of (a) experimentally measured $\Phi^{\text{expt}}_{\text{poly}}$ vs the computed $\bar{\Phi}$ and (b) $\Phi^{\text{expt}}_{\text{poly}}$ vs the computed $\Phi^{\text{lowest}}_{\text{hkl}}$. The single-factor linear regression line $y = x + c$ for both plots are indicated as dashed blue lines along with the R^2 value and standard error of the estimate (SEE). Values within the light blue (light yellow) region are below (above) the SEE. (see refs [5,38,39]). (For interpretation of the references to color in this figure legend, the reader is referred to the web version of this article.)

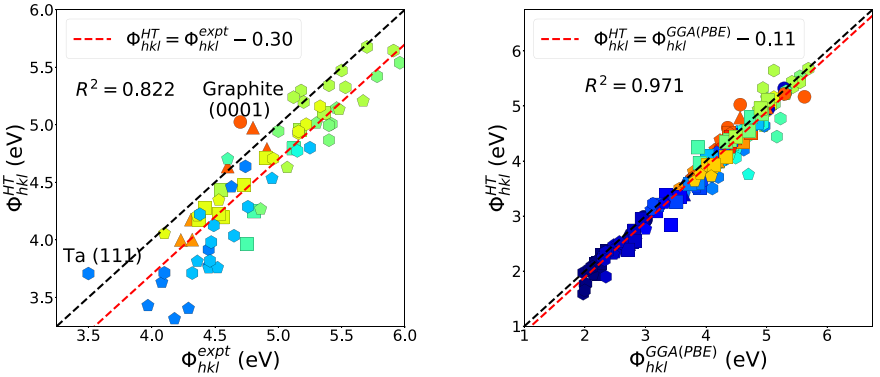

(a) Φ_{hkl} vs $\Phi^{\text{expt}}_{\text{hkl}}$ (literature). (b) Φ_{hkl} vs PBE (literature).

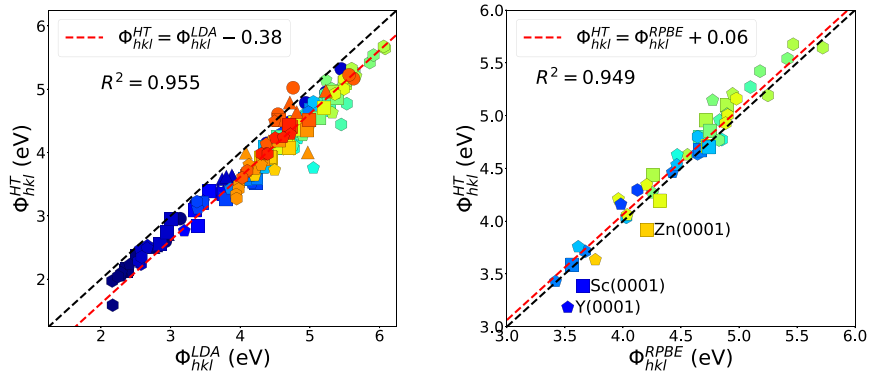

(c) Φ_{hkl} vs LDA (literature). (d) Φ_{hkl} vs RPBE (this study).

Fig. 4. Plot of computed facet-dependent $\Phi^{\text{HT}}_{\text{hkl}}$ in this work vs (a) experimental values [5,17,38] (b) literature PBE values [11,12,21,23], (c) literature LDA values [12,21,23] and (d) RPBE values (this work).

3.1.1. *Work function of missing-row reconstructions*

Fig. 5 compares the work function for the (110) missing-row reconstructed surface of face-centered cubic metals ($\Phi^{\text{recon}}_{110}$) to the work function of the corresponding unreconstructed surface ($\Phi^{\text{unrecon}}_{110}$). As found in our previous work, only Pt, Au and Ir have significantly lower surface energies for the (110) missing-row reconstruction compared to the unreconstructed surface, which is in agreement with experimental observations. In general, we find that reconstruction leads to a relatively small increase in the work functions, though the three fcc metals exhibiting a thermodynamic driving force to reconstruct also have the

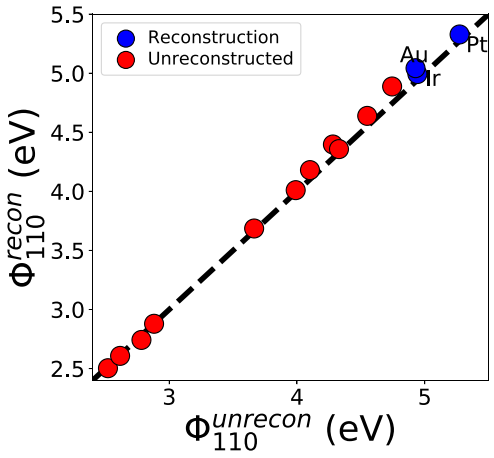

Fig. 5. Plot of the (110) work function for an unreconstructed ($\Phi_{110}^{unrecon}$) and 1×2 missing-row reconstructed (Φ_{110}^{recon}) surface for fcc materials. Data points corresponding to materials where reconstruction is thermodynamically favorable (-2 meVÅ$^{-2} < \gamma_{110}^{recon} - \gamma_{110}^{unrecon}$) are labelled in blue. (For interpretation of the references to color in this figure legend, the reader is referred to the web version of this article.)

largest work functions.

4. Discussion

4.1. Periodic trends in the work function

Fig. 6(a) plots $\bar{\Phi}$ against the periodic group number for transition metals which demonstrates a parabolic behavior with the position of the parabolic maxima located at group 10 (Pt group). When plotting $\bar{\Phi}$ against the weighted surface energy ($\bar{\gamma}$) in Fig. 6(b), we observe a split between elements above and below group 8. A similar parabolic trend when plotting $\bar{\gamma}$ against group number results in a maxima observed at group 7 rather than 10. The position of these parabolic peaks are related to the increasing cohesive energy resulting from the increasing number of half-filled *d*-orbitals as well as the width of the electronic *s, p* and *d* bands. For a more in-depth discussion, the interested reader is referred to the references here in [20,42]. We further note that cohesive energy and thus surface energy are strongly correlated with mechanical properties which suggests a cohesive energy origin to previously observed trends between $\bar{\Phi}$ and mechanical properties of transition metals [2,4,43].

To our knowledge, this work represents the first time DFT has been used to calculate the work functions of the lanthanides. Fig. 6(c) plots $\bar{\Phi}$ against the group number. A gradual decrease is observed for the half-filled lanthanides from Ce to Sm with a sharp decrease for Eu. The latter half of the lanthanides has a relatively constant value from Gd to Tm with a sharp decrease for Yb. Afterwards, a sharp increase is observed for Lu. These trends are consistent with trends of the cohesive energies of the lanthanides (see Fig. S2), which in turn may be attributed to the gradual filling of the 4*f* orbitals. The two lowest $\bar{\Phi}$ are observed when the 4*f* orbitals are half filled (Eu) and completely filled (Yb), and these two elements also have the lowest cohesive energy and melting point among the lanthanides. With the exception of Ce, the computed $\bar{\Phi}$ underestimates the experimental values of Φ_{poly}^{expt} for the lanthanides with a standard deviation of 0.136 eV from Ce to Yb (see Table S1).

4.2. Discrepancies in the comparisons

In general, our computed work functions are consistent with previous computational studies [11,21,23]. It is well known that the GGA(PBE) functional underestimates the intermediate range van der Waals (vdW) forces and Fermi energy while having no long-range vdW

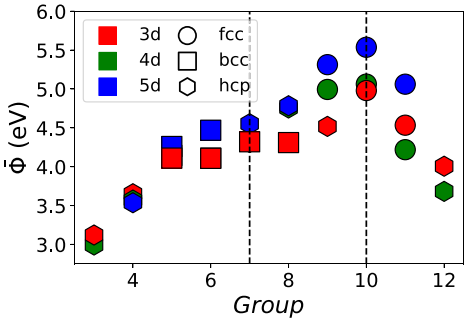

(a) Group number vs $\bar{\Phi}$ of transition metals.

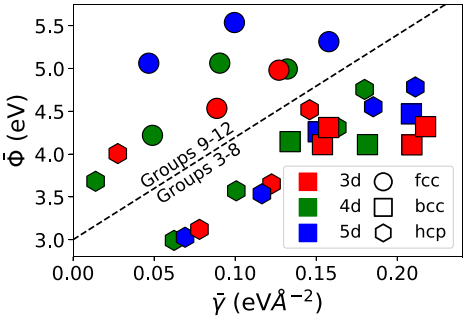

(b) $\bar{\gamma}$ vs $\bar{\Phi}$ of transition metals.

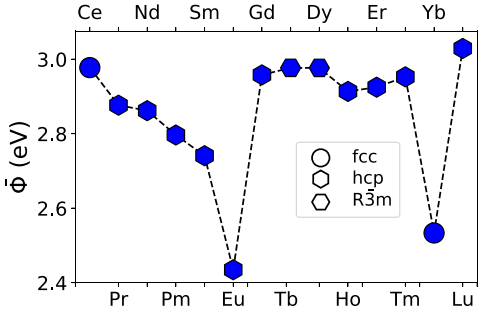

(c) Group number vs $\bar{\Phi}$ of Lanthanides.

Fig. 6. Plot of $\bar{\Phi}$ versus (a) group number and (b) $\bar{\gamma}$ for transition metals, and (c) $\bar{\Phi}$ versus group number for lanthanides. The left and right dashed lines in (a) corresponds to the parabolic peak when plotting group number against $\bar{\gamma}$ and $\bar{\Phi}$ respectively.

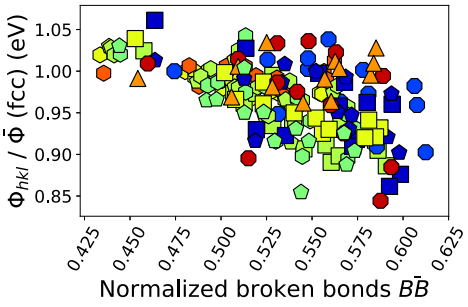

(a) $\Phi_{hkl}/\bar{\Phi}$ vs normalized broken bonds (fcc).

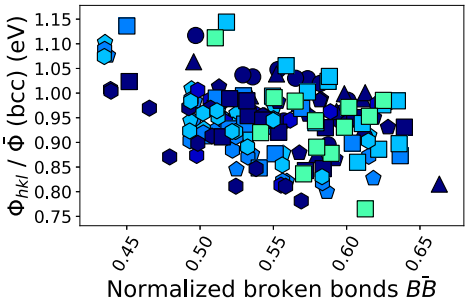

(b) $\Phi_{hkl}/\bar{\Phi}$ vs normalized broken bonds (bcc).

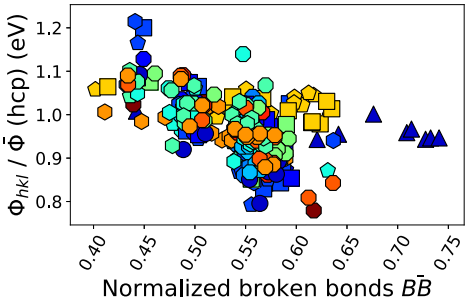

(c) $\Phi_{hkl}/\bar{\Phi}$ vs normalized broken bonds (hcp).

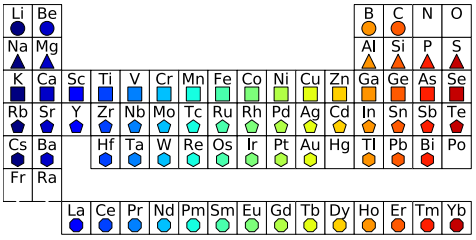

Fig. 7. Plot of the normalized broken bonds vs Φ_{hkl} normalized by average work function for (a) fcc, (b) bcc and (c) hcp structures for elemental crystalline solids commonly observed in literature. A legend indicating the element of each corresponding marker is shown at the bottom right.

forces, which generally leads to an underestimated work function. Although LDA generally yields values closer to experiment than GGA(PBE), this agreement is due to the various errors inherent in LDA that work in tandem to provide an error cancellation [23].

LDA/GGA are also known to have errors associated with overbinding/underbinding leading to smaller/larger cell volumes, lattice parameters and atomic distances, which can in turn influence surface properties. Larger atomic distances will decrease 2NN contributions to γ_{hkl} and Φ_{hkl}. This effect is especially prominent in the refractory metals Mo, Ta, Nb and W where the work function is shown to be dependent only on 1NN, but not 2NN (see Table S3). Without 2NN contributions, the work function will be severely underestimated in these metals when compared to experimental values, thus explaining the increasing deviation for refractory metals. Furthermore, the surface energy scales well with 2NN for Nb and Ta (which have the greatest deviation in Φ_{hkl} of the four refractory metals), indicating that underbinding in GGA(PBE) is more consequential for work function than it is for surface energy.

Experimental error is also a potential source of discrepancies in our comparisons. $\bar{\Phi}^{As}$ is significantly higher while $\bar{\Phi}^{La}$ and $\bar{\Phi}^{Se}$ are significantly lower than that of their corresponding values for Φ^{expt}_{poly}. Experimental values for these particular elements were taken from Michaelson [16] where surface contamination could lead to inaccuracies of up to 0.5 eV [7] in the reported measurements. Φ^{As}_{poly} is also known to range from 3.75 to 5.4 eV which our value for $\bar{\Phi}^{As}$ lies between. Furthermore, the value of Φ^{Se}_{poly} was also determined using a photoelectric method which is known to yield erroneous values of work function for semiconductors. In addition, we opted to use the latest values available from the literature, which for Φ^{La}_{poly} came from Michaelson [16], despite measurements from Rozkhov and Ye. [39] being 0.54 eV closer to our DFT and previous linear muffin-tin orbital method values [24].

Although the calculated Φ^{lowest}_{hkl} has previously been suggested as a good approximation of experimentally measured Φ^{expt}_{poly}, we have shown that the Wulff-area-weighted $\bar{\Phi}$ provides a much closer estimate. This suggests that the eclipsing effect of lower work functions in PES signals of patchy surfaces may not be as prominent as once thought. Despite this, the values of Φ^{expt}_{poly} are higher than $\bar{\Phi}$ by an average value of 0.18 eV. Kawano [5] has argued that the weighted work function is more likely to follow a Boltzmann distribution with a higher value than that provided by Eq. (2). In this context, temperature becomes an important factor in determining the work function [43,44]. However, it is unaccounted for in our calculations which are assumed to take place at 0 K.

4.3. Effect of reconstruction on work function

In general, the work function of the reconstructed facets are slightly larger than that of the unreconstructed facets. This can be due to the exposure of the {111} facets during reconstruction which generally have larger values of Φ_{hkl} than the (110) facet due to the lack of Smoluchowski smoothing in the flat {111} surfaces. It is not coincidental that the disparity between Φ^{recon}_{110} and $\Phi^{unrecon}_{110}$ for metals with surface reconstruction (Au, Ir, and Pt) is larger than for other metals. Ho and Bohnen [45] previously explained that missing row reconstruction was the result of competing forces that contributed to the kinetic energy (KE) contributions to surface energy. A missing-row introduces additional broken *d*-bonds for transition metals which increases KE. At the same time, a larger surface area is created from the newly exposed {111} facets which will better facilitate the spreading of *s* and *p* electrons. This increase in electron spreading will lower the

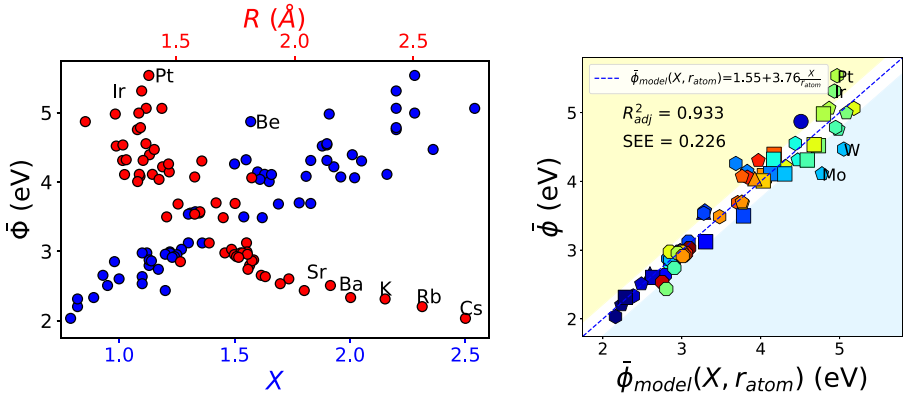

(a) $\bar{\Phi}$ vs χ and R (b) Improved model

Fig. 8. Plot for the calculated $\bar{\Phi}$ against (a) Pauling electronegativity χ and metallic radius R, and (b) predictions from improved model for $\bar{\Phi} = 1.55 + 3.76\frac{\chi}{r_{atom}}$, where $r_{atom} = \sqrt[3]{V_{atom}}$ and V_{atom} is the unit cell volume per atom.

surface KE and for some elements such as Au, Ir and Pt, is enough to overcome the KE increase. Recall that electron spreading will increase work function, a tenet of the Smoluchowski model (see later section), which explains the larger increase in Φ_{110}^{recon} for reconstructed surfaces relative to $\Phi_{110}^{unrecon}$.

4.4. Models for the work function

4.4.1. Smoluchowski rule

Fig. 7 plots Φ_{hkl} normalized by the average work function for each element $\bar{\Phi}$ as a function of the normalized broken bonds. All r values obtained from comparing Φ_{hkl} and γ_{hkl} to their respective normalized broken bonds and to each other are presented in Table S3. Strong negative correlations were observed for the anisotropic work functions of 23 metals: Au, Ni, Ag, Pd, Cu, Rh, Nb, Mo, Li, Ta, W, Y, Lu, Ru, Zr, La, Tc, Sc, Tm, Re, Eu, Er and Ho. Among these systems, similar trends have been confirmed in previous studies for Ni, Cu, Ag, Mo and W, but not for Au and Pd [5,11,21]. Ta and Nb are the only metals where a stronger correlation with surface energy ($r_{Ta} = 0.96$, $r_{Nb} = 0.88$) is observed when modelling with 2NN and work function ($r_{Ta} = -0.78$, $r_{Nb} = -0.86$) when modelling with 1NN. A moderate negative correlation is observed for 20 metals: Pt, Ir, Ca, Sr, Na, V, Cs, K, Cr, Mg, Ti, Zn, Pr, Hf, Tl, Co, Be, Nd, Sm and Os. The remaining 9 metals have weak negative correlations with Cd and Al having no negative correlation ($r_{Cd} = 0.01$, $r_{Al} = 0.22$) at all.

Grepstad et al. [41] has previously suggested that the Smoluchowski rule is valid only for systems with densely packed planes. It is well known that the c/a ratio of Cd is significantly larger than other hcp metals leading to sparsely packed planes along the (0001) direction [46] which can explain why Cd does not follow the Smoluchowski rule. However, although Grepstad et al. [41] was able to show that the computed values of Φ_{211}^{Cu} and Φ_{hkl}^{Al} are consistent with this explanation, our results clearly show that even for facets of Cu with MMI > 1, bond breaking trends are still valid.

Alternatively, Fall et al. [47] associates the anomalously low value of Φ_{111}^{Al} with the presence of p orbitals parallel to its surface which are highly favored in electronically dense facets. By decreasing the valence electrons at the surface, the p orbitals perpendicular to the surface become favored over the parallel p orbitals. This leads to an increase in Φ_{111}^{Al} that will eventually lead to an anisotropy consistent with the Smoluchowski rule. It is possible that the same phenomenon can explain the lack of correlation in other p-block systems such as Pb ($r = -0.05$).

4.5. An improved model for the work function of metals

The comprehensive data set presented in this work affords us the ability to develop more robust models for the work function of the elemental metals. It has previously been well-established by Michaelson [7] and Miedema et al. [8] that the work functions of metals have a positive linear relationship with the electronegativity χ of the metal. This may be explained by the fact that χ is a measure of how strongly electrons are bounded to the atom, and hence, the higher the χ, the greater the energy needed to bring an electron from the bulk to the free vacuum (Φ). Nevertheless, as can be seen from Fig. 8(a), it is clear that χ only explains $R^2 = 85.5\%$ of the variation in $\bar{\Phi}$ across the metals.

We carried an investigation of the relationship between $\bar{\Phi}$ and various atomic properties. As can be seen from Fig. 8(a), a strong, albeit non-linear, negative relationship is observed between $\bar{\Phi}$ and the metallic radius R. From Gauss' law, the potential inside an infinite charged plate is proportional to the bulk charge density times the square of the thickness of the plate, i.e., it scales charge per unit length of material. We postulate that the average work function is proportional to the electron density per unit length, similar in spirit to the traditional jellum work function model for metals [48]. We performed a linear regression of $\bar{\Phi}$ against $\frac{\chi}{r_{atom}}$, where χ is related to the electron charge contributed per atom (in line with previous models) and $r_{atom} = \sqrt[3]{V_{atom}}$, where V_{atom} is the unit cell volume per atom. As shown in Fig. 8(b), this optimized model $\bar{\Phi} = 1.55 + 3.76\frac{\chi}{r_{atom}}$ exhibits a much improved prediction accuracy for $\bar{\Phi}$, with a very high R^2 of 0.933 and a small SEE of 0.226 eV.

5. Conclusion

In conclusion we have constructed the largest database of anisotropic work functions to date. We have validated our database by comparing to both experimental and computational results from the literature and by confirming previously observed trends. In addition, we have also developed a technique for estimating the work function of a polycrystalline specimen using the Wulff shape and showed that it is a significantly more accurate estimate for experimental polycrystalline values than the lowest anisotropic work function. Using this large dataset, we have also extensively probed well-known empirical relationships for the work function, such as the Smoluchowski rule, and developed a substantially-improved prediction model for the work function of the metals from atomic properties such as the electronegativity and metallic radius.

Acknowledgment

This work is supported by the Materials Project, funded by the U.S. Department of Energy, Office of Science, Office of Basic Energy Sciences, Materials Sciences and Engineering Division under Contract no. DE-AC02-05-CH11231: Materials Project program KC23MP. The authors also acknowledge computational resources provided by Triton Shared Computing Cluster (TSCC) at the University of California, San Diego, the National Energy Research Scientic Computing Centre (NERSC), and the Extreme Science and Engineering Discovery Environment (XSEDE) supported by National Science Foundation under grant no. ACI-1053575.

Supplementary information

The accompanying Supplementary Information contains tables listing the values of all data points from the figures in this manuscript. It also contains the *r* values for a linear regression of anisotropic work functions versus the corresponding normalized broken bonds. Additional plots are also available to support the analysis presented in the main manuscript. Supplementary material associated with this article can be found, in the online version, at 10.1016/j.susc.2019.05.002

References

[1] G. Heimel, L. Romaner, J.L. Bredas, E. Zojer, Interface energetics and level alignment at covalent metal-molecule junctions: pi-conjugated thiols on gold, Phys. Rev. Lett. 96 (19) (2006) 2–5, https://doi.org/10.1103/PhysRevLett.96.196806. ISSN 00319007

[2] H. Lu, G. Hua, D. Li, Dependence of the mechanical behavior of alloys on their electron work function - an alternative parameter for materials design, Appl. Phys. Lett. 103 (26) (2013) 2619021–2619024, https://doi.org/10.1063/1.4852675. ISSN 00036951

[3] H. Lu, Z. Liu, X. Yan, D. Li, L. Parent, H. Tian, Electron Work Function - a Promising Guiding Parameter for Material Design, Nature Publishing Group, 2016, pp. 1–11, https://doi.org/10.1038/srep24366. ISSN 2045-2322

[4] G. Hua, D. Li, Electron work function: a novel probe for toughness, Phys. Chem. Chem. Phys. 18 (6) (2016) 4753–4759, https://doi.org/10.1039/C5CP04873G. ISSN 1463-9076

[5] H. Kawano, Effective work functions for ionic and electronic emissions from mono- and polycrystalline surfaces, Prog. Surf. Sci. 83 (2008) 1–165, https://doi.org/10.1016/j.progsurf.2007.11.001.

[6] T. Li, B.L. Rickman, W.A. Schroeder, Density functional theory analysis of hexagonal close-packed elemental metal photocathodes, Phys. Rev. Spec. Top. 18 (7) (2015) 1–11, https://doi.org/10.1103/PhysRevSTAB.18.073401. ISSN 10984402

[7] H.B. Michaelson, Relation between an atomic electronegativity scale and the work function, IBM J. Res. Dev. 22 (1) (1978) 72–80, https://doi.org/10.1147/rd.221.0072. ISSN 0018-8646

[8] A.R. Miedema, F.R. De Boer, P.F. De Chatel, Empirical description of the role of electronegativity in alloy formation, J. Phys. F 3 (8) (1973) 1558–1576, https://doi.org/10.1088/0305-4608/3/8/012. ISSN 0031899X,

[9] R. Smoluchowski, Anisotropy of the electronic work function of metals, Phys. Rev. 60 (9) (1941) 661–674, https://doi.org/10.1103/PhysRev.60.661.

[10] J. Sokolov, F. Jona, Trends in metal surface relaxation, Solid State Commun. 49 (4) (1984) 307–312.

[11] J. Wang, S.Q. Wang, Surface energy and work function of fcc and bcc crystals: density functional study, Surf. Sci. 630 (March) (2014) 216–224, https://doi.org/10.1016/j.susc.2014.08.017. ISSN 00396028

[12] D.P. Ji, Q. Zhu, S.Q. Wang, Detailed first-principles studies on surface energy and work function of hexagonal metals, Surf. Sci. 651 (2016) 137–146, https://doi.org/10.1016/j.susc.2016.04.007. ISSN 00396028

[13] I. Brodie, Uncertainty, topography, and work function, Phys. Rev. B 51 (19) (1995) 13660–13668, https://doi.org/10.1103/PhysRevB.51.13660. ISSN 01631829

[14] K.F. Wojciechowski, M. Borna, Work function of transition metals calculated from the Brodie's expression, Vacuum 48 (3) (1997) 257–259.

[15] F. Fazylov, Macroscopic theory of the electron work function in solids, Philos. Mag. 94 (17) (2014) 1956–1966, https://doi.org/10.1080/14786435.2014.903007. ISSN 1478-6435

[16] H.B. Michaelson, The work function of the elements and its periodicity, J. Appl. Phys. 48 (11) (1977) 4729–4733, https://doi.org/10.1063/1.323539. ISSN 00218979

[17] G.N. Derry, M.E. Kern, E.H. Worth, Recommended values of clean metal surface work functions, J. Vacuum Sci. Technol. A 33 (6) (2015) 060801, https://doi.org/10.1116/1.4934685.

[18] M.G. Helander, M.T. Greiner, Z.B. Wang, Z.H. Lu, Pitfalls in measuring work function using photoelectron spectroscopy, Appl. Surf. Sci. 256 (2010) 2602–2605, https://doi.org/10.1016/j.apsusc.2009.11.002.

[19] N.E. Singh-Miller, N. Marzari, Surface energies, work functions, and surface relaxations of low-index metallic surfaces from first principles, Phys. Rev. B 80 (23) (2009), https://doi.org/10.1103/PhysRevB.80.235407. ISSN 10980121

[20] M. Methfessel, D. Hennig, M. Scheffler, Trends of the surface relaxations, surface energies, and work functions of the 4d transition metals, Phys. Rev. B 46 (8) (1992) 4816–4829, https://doi.org/10.1103/PhysRevB.46.4816. ISSN 0163-1829

[21] S.D. Waele, K. Lejaeghere, M. Sluydts, S. Cottenier, Error estimates for density-functional theory predictions of surface energy and work function, Phys. Rev. B 94 (2016) 1–13, https://doi.org/10.1103/PhysRevB.94.235418.

[22] H.L. Skriver, N.M. Rosengaard, Surface energy and work function of elemental metals, Phys. Rev. B 46 (11) (1992) 7157–7168, https://doi.org/10.1103/PhysRevB.46.7157. ISSN 01631829

[23] A. Patra, J. Bates, J. Sun, J.P. Perdew, Properties of real metallic surfaces: Effects of density functional semilocality and van der Waals nonlocality, Arxiv (2017) 1–17.

[24] T. Durakiewicz, A. Arko, J.J. Joyce, D.P. Moore, S. Halas, Electronic work-function calculations of polycrystalline metal surfaces revisited, Phys. Rev. B 64 (4) (2001) 1–8, https://doi.org/10.1103/PhysRevB.64.045101. ISSN 1550235X

[25] M. Aldén, B. Johansson, H.L. Skriver, Surface shift of the occupied and unoccupied 4f levels of the rare-earth metals, Phys. Rev. B 51 (8) (1995) 5386–5396, https://doi.org/10.1103/PhysRevB.51.5386. ISSN 01631829

[26] a.A. Stekolnikov, J. Furthmuller, F. Bechstedt, J. Furthmüller, F. Bechstedt, Absolute surface energies of group-IV semiconductors: dependence on orientation and reconstruction, Phys. Rev. B 65 (11) (2002) 115318, https://doi.org/10.1103/PhysRevB.65.115318. ISSN 0163-1829

[27] T.A. Delchar, Modern Techniques of Surface Science, Third ed., Cambridge University Press, Cambridge, 1986.

[28] R. Tran, Z. Xu, B. Radhakrishnan, D. Winston, W. Sun, K.A. Persson, S.P. Ong, Data descripter: surface energies of elemental crystals, Sci. Data 3 (160080) (2016) 1–13, https://doi.org/10.1038/sdata.2016.80. ISSN 0929-1903

[29] F.C. Frank, J.S. Kasper, Complex alloy structures regarded as sphere packings. i. definitions and basic principles, Acta Crystallographica 11 (1958) 184–190, https://doi.org/10.1107/S0365110X58000487.

[30] W. Sun, G. Ceder, Efficient creation and convergence of surface slabs, Surf. Sci. 617 (2013) 53–59, https://doi.org/10.1016/j.susc.2013.05.016. ISSN 00396028

[31] J.H. Montoya, K.A. Persson, A high-throughput framework for determining adsorption energies on solid surfaces, npj Comput. Mater. 3 (1) (2017) 14, https://doi.org/10.1038/s41524-017-0017-z. ISSN 2057-3960

[32] S.P. Ong, W.D. Richards, A. Jain, G. Hautier, M. Kocher, S. Cholia, D. Gunter, V.L. Chevrier, K.A. Persson, G. Ceder, Python materials genomics (pymatgen): a robust, open-source python library for materials analysis, Comput. Mater. Sci. 68 (2013) 314–319, https://doi.org/10.1016/j.commatsci.2012.10.028. ISSN 09270256

[33] A. Jain, S.P. Ong, W. Chen, B. Medasani, X. Qu, M. Kocher, M. Brafman, G. Petretto, G.M. Rignanese, G. Hautier, D. Gunter, K.A. Persson, Fireworks: a dynamic workflow system designed for high-throughput applications, Concurr. Comput. 27 (17) (2015) 5037–5059, https://doi.org/10.1002/cpe.3505. ISSN 15320634

[34] K. Mathew, J.H. Montoya, A. Faghaninia, S. Dwarakanath, M. Aykol, H. Tang, I.-h. Chu, T. Smidt, B. Bocklund, M. Horton, J. Dagdelen, B. Wood, Z.-k. Liu, J. Neaton, S. Ping, K. Persson, A. Jain, Atomate : a high-level interface to generate, execute, and analyze computational materials science workflows, Comput. Mater. Sci. 139 (2017) 140–152, https://doi.org/10.1016/j.commatsci.2017.07.030. ISSN 0927-0256

[35] D. Winston, J.H. Montoya, K.A. Persson, Interactive leaderboard for requesting and tracking expensive calculations of optional properties across a database of materials, 11th Gateway Computing Environments Conference, (2016), https://doi.org/10.6084/m9.figshare.4491623.v2.

[36] Crystalium, 2016, (http://crystalium.materialsvirtuallab.org/).

[37] The materials project, 2015, (https://materialsproject.org/).

[38] W.M. Haynes, D.R. Lide, T.J. Bruno, CRC handbook of chemistry and physics, Ninty seventh ed., CRC Press, Boca Raton, Fl, 2017.

[39] O.K.K. Rozkhov, E. Ye., Rare Earth Metals and Alloys, Nauka, Moscow, 1971.

[40] R.M. Eastmen, C.H.B. Mee, Work function measurements on (100), (110) and (111) surfaces of aluminium, J. Phys. F 3 (March) (1973) 1738–1745.

[41] J. Grepstad, P. Gartland, B. Slagsvold, Anisotropic work function of clean and smooth low-index faces of aluminium, Surf. Sci. 57 (July) (1976) 348–362.

[42] A. Michaelides, M. Scheffler, An introduction to the theory of metal surfaces,...of Surface and Interface Science(2010) 1–40.

[43] R. Rahemi, D. Li, Variation in electron work function with temperature and its effect on the Young's modulus of metals, Scripta Materialia 99 (2015) 41–44, https://doi.org/10.1016/j.scriptamat.2014.11.022. ISSN 13596462

[44] A. Kiejna, K.F. Wojciechowski, J. Zebrowksi, The temperature dependence of metal work functions, J. Phys. F 9 (7) (1979) 1361, https://doi.org/10.1088/0305-4608/9/7/016. ISSN 0305-4608

[45] K.M. Ho, K.P. Bohnen, Stability of the missing-row reconstruction on fcc (110) transition-metal surfaces, Phys. Rev. Lett. 59 (16) (1987) 1833–1836, https://doi.org/10.1103/PhysRevLett.59.1833. ISSN 00319007

[46] N. Gaston, D. Andrae, B. Paulus, U. Wedig, M. Jansen, Understanding the hcp anisotropy in cd and zn: the role of electron correlation in determining the potential energy surface, Phys. Chem. Chem. Phys. 12 (3) (2010) 681–687, https://doi.org/10.1039/B915967C. ISSN 1463-9076 http://xlink.rsc.org/?DOI=B915967C

[47] C.J. Fall, N. Binggeli, A. Baldereschi, Anomaly in the anisotropy of the aluminum work function, Phys. Rev. B 58 (12) (1998) R7544–R7547, https://doi.org/10.1103/PhysRevB.58.R7544.

[48] N.D. Lang, W. Kohn, Theory of metal surfaces: work function, Phys. Rev. B 3 (4) (1971) 1215–1223, https://doi.org/10.1103/PhysRevB.3.1215. http://link.aps.org/doi/10.1103/PhysRevB.3.1215